In situ Growth of Silver Nanoparticles in Porous Membranes for Surface-Enhanced Raman Scattering

Sehoon Chang, Zachary A. Combs, Maneesh K. Gupta, Richard Davis, and Vladimir V. Tsukruk*

School of Materials Science and Engineering, Georgia Institute of Technology, Atlanta, Georgia, United States

ABSTRACT We demonstrate the in situ growth of silver nanoparticles in porous alumina membranes (PAMs) for use as a surface-enhanced Raman scattering (SERS) detection substrate. This fabrication method is simple, cost-effective, and fast, while providing control over the size of silver nanoparticles through the entire length of the cylindrical nanopores with uniform particle density inside the pores unachievable by the traditional infiltration technique. The in situ growth of silver nanoparticles was conducted from electroless-deposited nanoscale seeds on the interior of the PAM and resulted in the formation of numerous hot spots, which facilitated significantly higher SERS enhancement for these substrates compared with previously reported porous substrates.

KEYWORDS: silver nanoparticle • surface-enhanced Raman scattering • nanoparticle assembly • porous alumina membrane • electroless deposition

INTRODUCTION

Surface-enhanced Raman scattering (SERS) is considered to be one of the most powerful analytical techniques for the detection of chemical and biological analytes because of its high sensitivity, selectivity, rapid response, and prospective portability (1). Raman enhancement occurs when molecules are adsorbed at the interstices between adjacent metal nanoparticles called hot spots (2−5 nm interparticle gaps) due to the strong electromagnetic field associated with the surface plasmon resonance of metal nanostructures (2, 3). This interparticle plasmon coupling is extremely important for the intense enhancement of the SERS signal from molecules adsorbed at the nanoparticle junctions, providing the capability for single molecule detection (4). Therefore, the design of well-defined metal nanostructures to maximize the number of hot spots is the most critical aspect to consider in SERS sensor design (5). To date, numerous studies have been reported on the design of 1D and 2D SERS substrates utilizing metallic and bimetallic nanostructure arrays by precisely controlling the size of nanoparticles and interparticle distances (6−14).

For practical applications of SERS-active substrates, the sensitivity of planar metal structures remains modest due to the limited concentration of hot spots available within the laser-activated footprint. To overcome this obstacle, 3D SERS substrates with advantages including large surface area to maximize the number of hot spots and sites for adsorption of analyte molecules have been demonstrated to have high enhancement. For example, silver nanostructures in the form of nanowires, nanosheets, and nanoplates have been suggested for SERS substrates (8, 14−16). Recently, silver nanorod arrays have been designed as SERS substrates using oblique angle vapor deposition (17). However, these and other random-organized surface structures show limited enhancement, limited mechanical strength, and cannot be easily adapted for microfluidic and stand alone designs. On the other hand, device-friendly and robust designs such as micro-optical fibers were combined with metal nanoparticles for efficient 3D SERS substrates (18, 19). Porous membranes with cylindrical nanopores infiltrated with metal nanoparticles have also been introduced as substrates with high enhancement that is much higher than conventional planar SERS substrates (20). These substrates can be easily modified for SERS activity, readily reproduced, show excellent mechanical strength and flexibility, cost-effective, and can be easily adapted to microfluidic-based and vapor-flow Raman-detection devices.

However, the critical challenge of using these porous membrane substrates or the long hollow microfibers for efficient SERS detection is the difficulty of filling nanosized cylindrical pores with large amount of metal nanoparticles without clogging these nanostructures with usual pore diameter within 100−200 nm. The limited mass transport throughout the continuous microscopic channels requires a channel diameter of several micrometers, which ultimately decreases their efficiency because of the low specific density of hot spots (21, 22). Even though these SERS substrates have shown decent sensitivities, the fabrication method itself is costly and requires multiple complicated steps.

The largest Raman enhancement occurs when the absorption band of the metallic nanostructures is located near the wavelength of the incident laser of the Raman detection setup being used (23). By tuning the surface plasmon resonance of the nanoparticles (by variation in the shape,

* Corresponding author. E-mail: vladimir@mse.gatech.edu.
Received for review August 18, 2010 and accepted October 14, 2010
DOI: 10.1021/am100758k

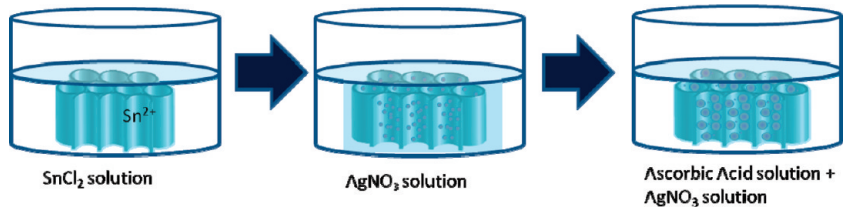

FIGURE 1. In situ growth of silver nanoparticles from electroless-deposited seeds in PAMs utilized in this study.

size, composition, and aggregation), very strong localized fields can be achieved at a predetermined wavelength (24−26). Because silver nanoparticles are considered to be an efficient plasmonic material, they have been widely used as a nanostructure assembly for SERS substrates despite their questionable long-term stability due to modest oxidation (27). Recently, a well-ordered array of silver nanoparticles grown from gold seeds on a block copolymer template was demonstrated as a possible SERS substrate (28). However, these and other planar SERS substrates possess a limited concentration of hot spots and some methods require additional plasma etching or other roughening steps.

Here, we have demonstrated the integration of silver nanoparticles by an in situ growth method from electroless-deposited seeds within well-defined porous alumina membranes (PAMs). Thin PAMs with vertical cylindrical pores have already been utilized for the fabrication of 3D silver nanostructure arrays with controlled size and interparticle distance for SERS substrates (29, 30). Our previous study demonstrated PAMs decorated with gold nanoparticles which were fabricated as robust and facile SERS substrates utilizing polyelectrolytes to bind the gold nanoparticles by a vacuum infiltration method (20, 31).

Compared to this previous approach, the fabrication method introduced here excludes the adhesive polymer layer, which prevents possible overlap of the Raman bands of the polymer and analyte molecules. Moreover, the in situ seed growth of silver nanoparticles from very fine electroless-deposited nanoseeds is simple, cost-effective, and provides a uniform density of nanoparticles along the cylindrical nanopores. This is in contrast with the vacuum infiltration method, which frequently results in the deposition of larger nanoparticles predominantly in the proximity of the top of the PAM surface and with reduced concentration at the bottom of the membrane. The silver nanoparticle-decorated SERS substrates provided efficient interaction between the excitation light source and silver nanoparticle aggregates dispersed on the inner walls of the PAM when the incident light passed through the cylindrical channel. As the light passes through the channels, multiple reflections can occur resulting in a higher probability of interactions with "hot spots" compared to planar SERS substrates resulting in uniform and efficient SERS properties throughout the entire thickness of the PAM structures (32, 33).

RESULTS AND DISCUSSION

Fabrication of 3D SERS Substrate with Silver Nanoparticles and PAMs. Silver seeds were immobilized inside PAMs by electroless deposition as shown in Figure 1. Silver nanoparticles with very small sizes were uniformly immobilized along the interior walls of the pores of the PAM by a simple electroless deposition method (34). The PAM was immersed in an aqueous mixture of $SnCl_2$ and HCl resulting in the deposition of Sn^{2+} on the pore walls. The PAM was then soaked in aqueous $AgNO_3$ solution to reduce silver seeds on the pore walls. This was completed via the reduction of silver on the surface of the pore walls using the following reduction reaction 1 from the salt solution which penetrates through all of the pores (34).

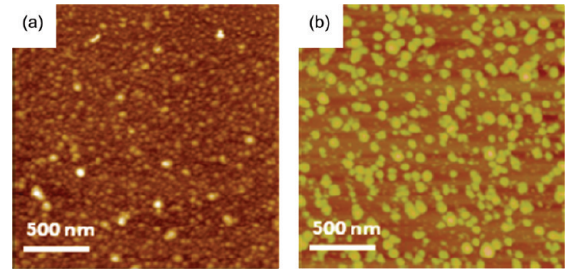

FIGURE 2. (a) AFM images of the electroless-deposited seeds (*Z* scale =50 nm) and (b) the silver nanoparticles grown from the seeds (*Z* scale =100 nm).

$$Sn^{2+}(aq) + 2Ag^{+} \rightarrow Sn^{4+}(aq) + 2Ag(s) \qquad (1)$$

The silver seed deposition cycle was repeated three times to provide a high density of silver seed particles on the pore walls, which was required for the subsequent in situ growth of silver nanoparticles.

In situ growth of larger silver nanoparticles was employed to complete the controlled assembly of properly-sized silver nanoparticles on the interior walls of the 3D SERS substrates (35). Following the electroless deposition of silver seeds on the interior surfaces of the pores of the PAM, large and highly concentrated silver nanoparticles were formed through a heterogeneous nucleation and growth mechanism.

First, to elucidate the nanostructured morphologies, we conducted AFM scanning to show the size and degree of aggregation of the seeds and corresponding silver nanoparticles formed by in situ growth from electroless-deposited seeds grown on model planar silicon substrate (Figure 2). The results of the cross-sectional analysis showed the average size of silver seeds to be about 7 ± 2 nm. When the substrate was exposed to the nanoparticle growth solution, larger silver nanoparticles can be formed with a diameter of several tens of a nanometer as illustrated in Figure 2b and can be controlled by the kinetics conditions (see below).

As known, the nucleation and growth process is dependent on several factors including the free energy of the

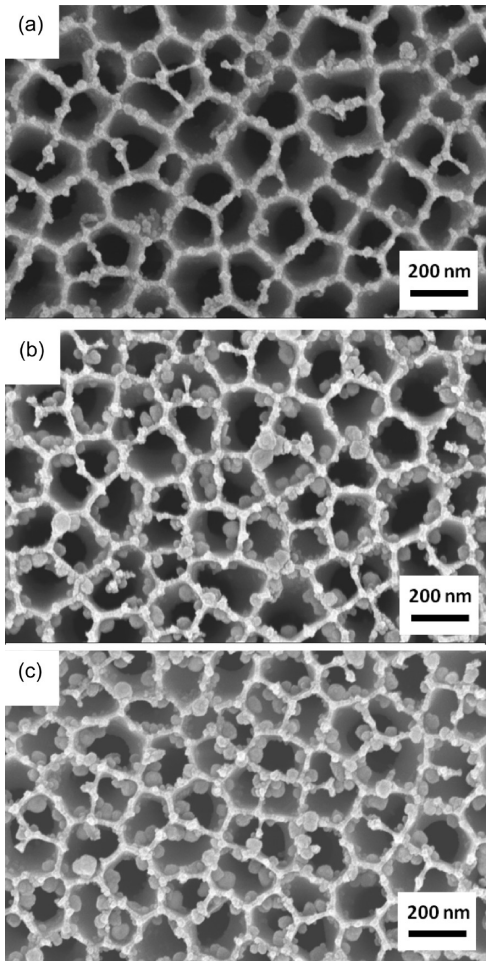

FIGURE 3. Top view SEM images of time dependent in situ growth of silver nanoparticles from electroless-deposited seeds in PAMs. (a) 10 min (b) 20 min, and (c) 30 min of growth time of silver nanoparticles from electroless-deposited silver seed in PAMs.

different phases, the concentration of nuclei and growth species in solution, and the surface energy of the growing particles (36). For homogeneous growth, the growth step is limited only by the diffusion of growing species in the growth media to the surface of the growing particle (37). In this way, the preliminary seeded wall regions provide controlled growth of silver nanoparticles on the inner pore surface based on the concentration of growth species provided in the solution. Therefore, we investigated the actual size of the silver nanoparticles grown within the pores of the PAM.

The size of the silver nanoparticles grown inside PAM substrates was controlled by the time of particle growth at a fixed concentration of growth media. The changes in morphologies were monitored by SEM to understand the kinetics of nanoparticle growth under confined pore conditions. The SEM images show the time-dependence of the in situ growth of silver nanoparticles from electroless-deposited seeds inside the PAM template following exposure to a growth solution (an aqueous mixture of $AgNO_3$ and ascorbic acid) (Figures 3 and 4) (35). The top-view through the cylindrical pores as well as the internal view of pores on fractured PAMs are presented to show the distribution of silver nanoparticles in different parts of the membrane.

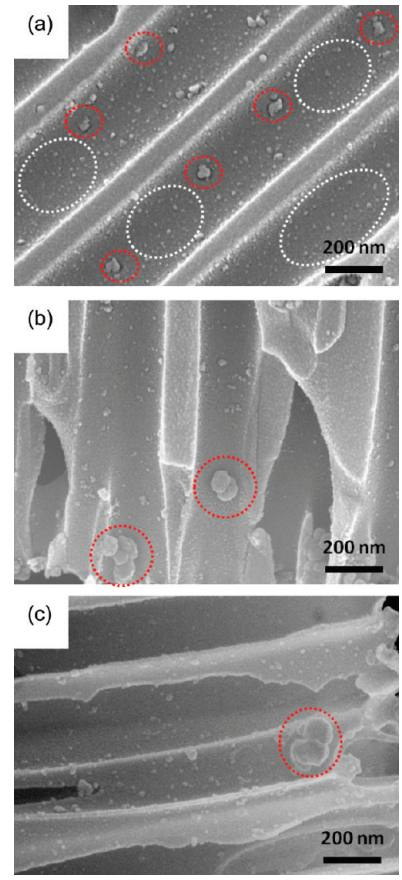

FIGURE 4. Cross-sectional SEM images of time-dependent in situ growth of silver nanoparticles from electroless-deposited seeds in PAMs. (a) 10 min (b) 20 min, and (c) 30 min of growth time of silver nanoparticles from electroless-deposited silver seed in PAMs. Electroless-deposited silver nuclei are marked with white ellipses and in situ grown silver nanoparticles are marked with red circles.

As clear from these images, solution growth for 10 min generates fairly small nanoparticles with a diameter of 20 $\pm$ 5 nm silver nanoparticles (Figures 3a and 4a). The energy-dispersive X-ray spectrum (EDS) of the SERS substrate confirms the presence of silver nanoparticles inside the PAM substrates (Figure 5). It was observed that allowing more time for silver nanoparticle growth resulted in a gradual increase in the size of the nanoparticles formed inside the PAM mostly within the initial 30 min; 40 $\pm$ 10 nm silver nanoparticles were uniformly formed on the wall of PAM after 20 min of growth as shown in Figures 3b and 4b. Finally, 60 $\pm$ 10 nm silver nanoparticles were obtained after 30 min of growing in solution (Figures 3c and 4c). At longer times, the size of nanoparticles increased beyond the useful limit for SERS and these larger (>70 nm) nanoparticles clogged the pores with the average diameter of about 240 nm.

Raman Enhancement of 3D Controlled Assembly of Silver Nanoparticles. To measure the SERS activity of silver nanoparticles decorating the PAMs at various in situ growth times, an aqueous solution of 1×10^{-5} M Rhodamine 6G (R6G) was deposited on each SERS substrate (Figure 6). For Raman measurement, an excitation laser source of 514 nm was employed due to the plasmon absorption of the PAM substrates containing silver nanopar-

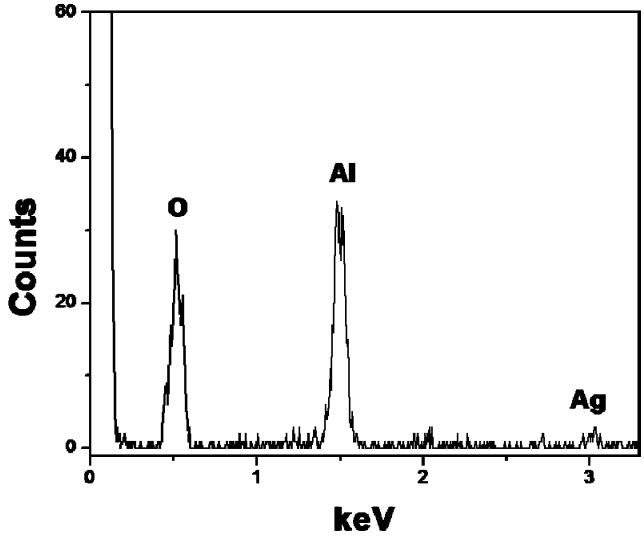

FIGURE 5. EDS spectrum of porous alumina membrane with grown silver nanoparticles.

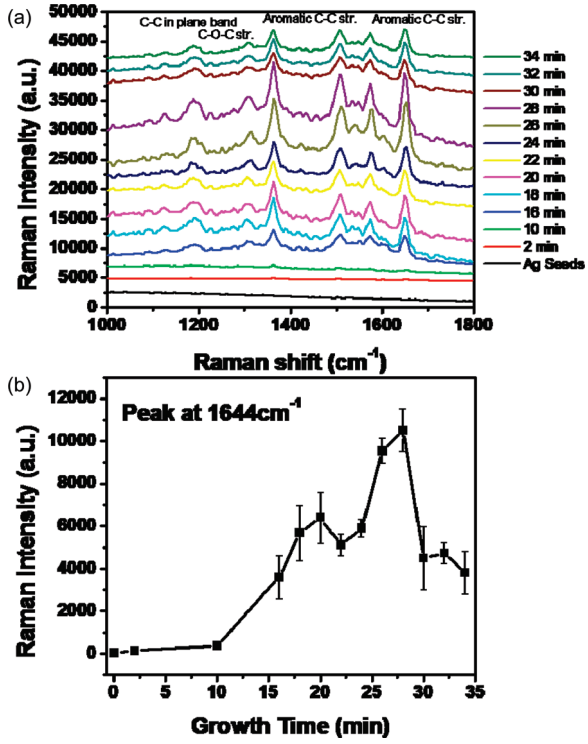

FIGURE 6. (a) Raman spectra of R6G on silver nanoparticles/PAM at various silver nanoparticle growing periods, (b) relative Raman intensity of 1644 cm^{-1} at different nanoparticle growth times.

ticles. These substrates are expected to provide strong SERS enhancement because the coupled plasmon resonance of the aggregated silver nanoparticles nearly overlaps with the wavelength of the excitation laser.

From the comparison of relative Raman intensities of each SERS substrate, the substrate containing silver nanoparticles grown for 25−30 min was observed to provide the largest SERS enhancement (Figure 6). Under these conditions, silver nanoparticles with diameters of 40−60 nm were grown inside PAM pores and utilized for further studies. The plasmon resonance properties of spherical metal nanoparticles are dependent on their size and level of aggregation,

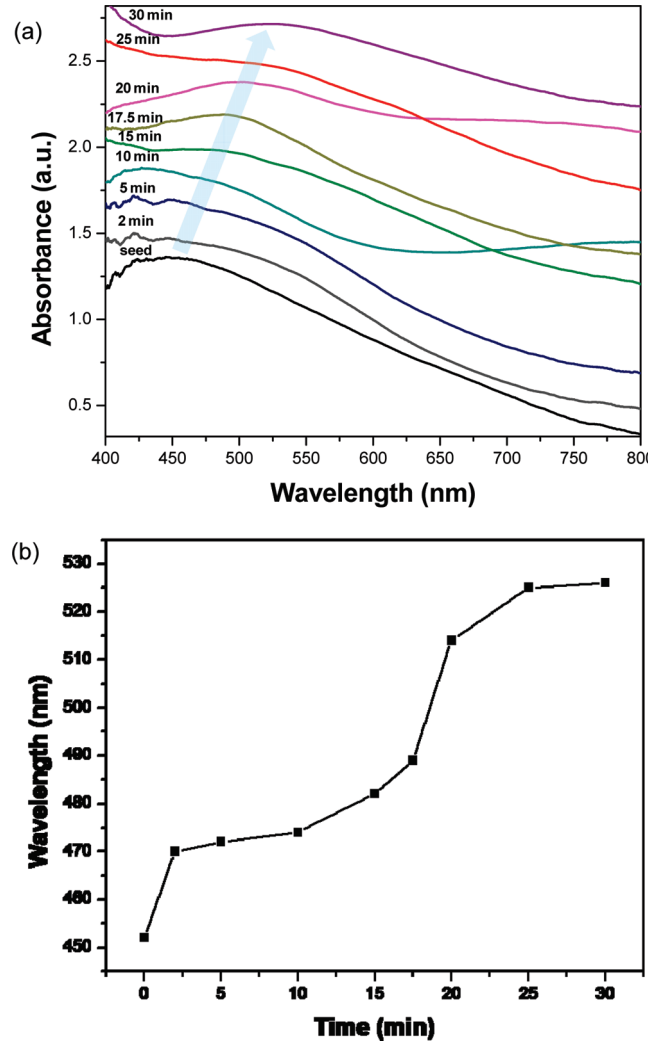

FIGURE 7. (a) Several representative UV−vis absorption spectra of in situ growth of silver nanoparticles from electroless deposited seeds in PAMs, (b) UV−vis absorption peaks of SERS substrates at different nanoparticle growth times.

thus controlling the size of silver nanoparticle is critical for SERS enhancement because the enhancement effect is highly localized and decays rapidly as the interparticle distance increases (38, 39). The aggregated silver nanoparticles of 40−60 nm on the SERS substrate were found to provide the optimum conditions for the largest SERS enhancement.

Optical Properties of Silver Nanoparticle PAMs.

Higher SERS enhancement can be achieved when the coupled plasmon resonance of the aggregated silver nanoparticles assembled in the PAMs overlaps with the wavelength of the excitation light (40). Thus, UV−vis absorption spectra were collected from several different substrates fabricated with various nanoparticle growth times. As shown in panels a and b in Figure 7, the growth of the silver nanoparticles resulted in a higher degree of aggregation of silver nanoparticles, which has been shown to cause a red shift of the plasmon band (41−43). The UV−vis absorption spectrum of the SERS substrate which contained silver nanoparticles grown for about 28 min shows an absorption band around 514 nm, which is close to the wavelength of the incident light. This

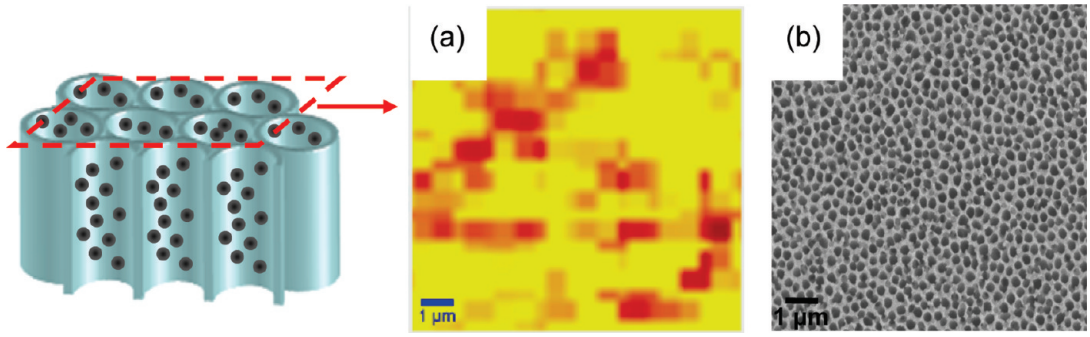

FIGURE 8. (a) Raman mapping of the 1644 cm^{-1} peak (R6G) in the lateral direction over a 10 μm × 10 μm area of the PAM and (b) corresponding SEM image. The range of relative Raman signal intensity, $Z = 0-1400$ au.

average size was selected because as has been shown for the absorption band of metallic nanostructures close to the wavelength of the exciting light, the largest Raman enhancement occurs (23).

As the silver nanoparticle size increased as discussed above, the plasmon band of the aggregated structures shifted closer toward the excitation wavelength, which corresponded to an increase of the measured SERS enhancement. When the silver nanoparticles were grown for more than 28 min, the UV−vis absorption spectra were red-shifted to wavelengths longer than that of the incident light (Figure 7a, b). Therefore, a decrease in the SERS enhancement should be expected under these conditions. As a result, this specific growth time under our fabrication conditions provides optimum nanoparticle densities, level of aggregation of nanoparticles, and plasmon band position for maximum SERS enhancement and thus was exploited for SERS studies.

SERS Characteristics of PAMs. To show the uniformity of the SERS phenomenon over a large area of the 3D assembled silver nanoparticles in the PAMs, Raman mapping of the SERS intensity was conducted using a well-known Raman analyte, Rhodamine 6G (R6G) (44). To conduct these measurements, the SERS substrates were immersed in an aqueous solution of 1×10^{-5} M R6G, rinsed thoroughly with Nanopure water, and SERS spectra of the substrates were collected. Characteristic Raman bands of R6G (1360, 1504, and 1644 cm^{-1}) from aromatic benzene rings were strongly enhanced by the silver nanoparticle PAM (Figure 6) (45). The intensity of Raman band at 1644 cm^{-1} was mapped all over the surface (x, y) and through the entire depth (z) of the PAM.

The 10 μm × 10 μm (x, y) mapping of the relative intensity of the 1644 cm^{-1} Raman band of R6G indicates that relatively uniform SERS enhancement occurs over the large area of the substrate with modest deviations in SERS intensity not exceeding ± 30% with a 1 s acquisition time and pixel size below 200 nm (Figure 8). It can be seen that there are brighter areas on the mapped surface as shown in Figure 8a, indicating that the aggregation of several nanoparticles on the surface can cause a greater SERS enhancement in some areas. However, most of the mapped surface appears bright on the SERS substrate, indicating that SERS enhancement occurs consistently over the entire large area.

To observe the SERS intensity through the pores of the 3D assembled silver nanoparticles within the PAM substrate,

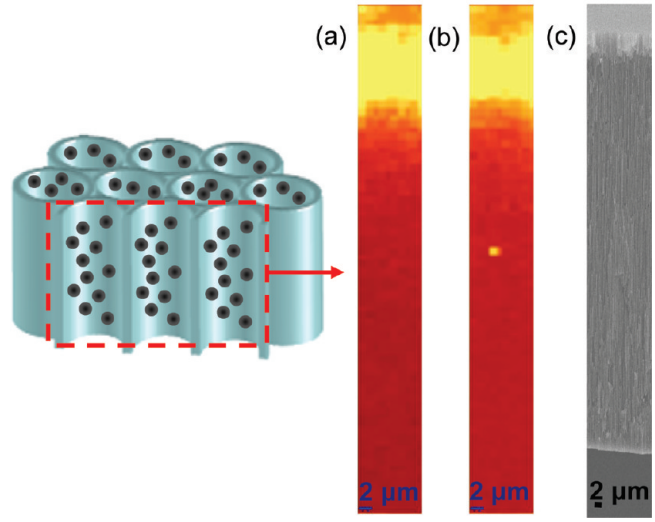

FIGURE 9. Raman mapping of the 1644 cm^{-1} peak in the Z-direction over a 10 μm × 80 μm area of PAMs. The range of relative Raman signal intensity, $Z = 0-600$ au.

we conducted Raman mapping in the z direction as well with a 0.5 s acquisition time (Figure 9). It is worth noting that both sides of the PAM were mapped because the commercial PAM utilized in this study has varying pore wall thickness (about 10 nm difference) on each side of the membrane (Figure 9). The largest SERS enhancement was observed in the first 20 μm in depth from the surface on both sides of the SERS substrate (Figure 9a,b). The Raman signal intensity of R6G from the SERS substrate fades after a depth of 20 μm from the surface. SERS intensity distribution was only slightly affected by the slight difference in the pore wall thickness (Figure 9). We suggest that this phenomenon can be attributed to the absorption of the incident laser light inside the PAM channel more than 20 μm in depth from the surface effectively decreasing the SERS enhancement through the channel (46).

To compare the Raman enhancement of the SERS substrate fabricated by the in situ growth of silver nanoparticles with a SERS substrate fabricated by the vacuum infiltration of silver nanoparticles combined with a polyelectrolyte binding layer (20), we deposited the same volume of R6G solution (with 1×10^{-5} M concentration) on both SERS substrates and conducted comparative SERS measurements under identical conditions.

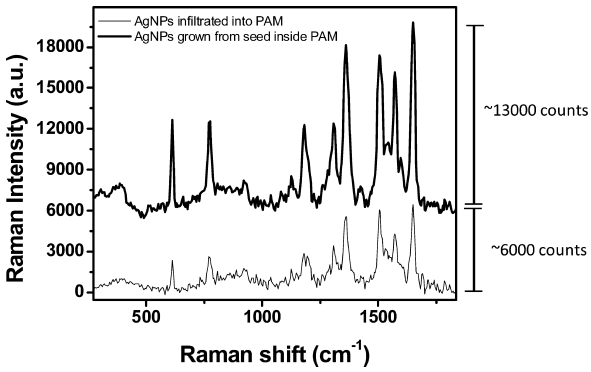

FIGURE 10. Raman spectra of R6G on PAM with in situ grown and conventional vacuum infiltrated silver nanoparticles.

As can be concluded from this direct comparison, the SERS substrate fabricated via the in situ growth of silver nanoparticles within the PAM showed almost twice as strong of Raman enhancement compared to the SERS substrate fabricated by vacuum infiltration (Figure 10). This significant increase indicates that the fabrication method of in situ growth introduced here can generate a more uniform silver nanoparticle distribution along the 3D channels of the PAMs resulting in increased SERS enhancement. The fabrication of large areas of SERS substrates by the in situ growth method is simpler and faster than by the vacuum infiltration method (46). Also, SERS substrates fabricated by the in situ growth of silver nanoparticles do not include a polyelectrolyte binding layer, which can be better for sensing applications because it is not necessary to separate the Raman bands of the polyelectrolyte binding layer from those of the desired analyte.

Finally, we conducted preliminary observations of long-term stability of our SERS PAM structures and their prospective shelf life under ambient laboratory conditions with more rigorous research for different storage conditions to be conducted in forthcoming studies. In this study, PAM substrates were stored in a sealed vial and their SERS properties were tested after different shelf times. This preliminary testing demonstrated that SERS activity of substrates is mostly preserved within 2 weeks after substrate preparation, which indicates slow oxidation of silver nanoparticles confined inside PAM nanopores.

CONCLUSIONS

In conclusion, we have demonstrated an efficient way to assemble silver nanoparticles within PAMs without clogging by taking advantage of uniformly deposited silver seeds from the electroless deposition method for use as an efficient SERS substrate. The silver nanoparticle-decorated porous structures with high concentration and uniform distribution of nanoparticles were fabricated by a simple and fast method, which provided uniformly controlled size of silver nanoparticles over the large surface area of the interior pore walls of the PAMs. In situ grown silver nanoparticles were assembled to provide the optimal size of the nanoparticles necessary for large SERS enhancement. The SERS enhancement and optical properties of the silver nanoparticle-decorated PAMs can be controlled by growth conditions in the PAM nanopores. These silver nanoparticle-filled cylindrical pores can be utilized as promising SERS substrates by taking advantage of the efficient light interaction with uniformly distributed nanoparticles along the interior walls of the PAMs. This method might allow future facile fabrication of seed grown nanorods, nanoplates, or nanocubes under tight physical confinement for advanced SERS applications, as will be explored in forthcoming studies.

EXPERIMENTAL SECTION

Electroless Deposition of Silver Seed Nanoparticles Inside Porous Alumina Membranes (PAMs). Silver nanoparticles were immobilized on the pore walls of PAMs (purchased from Whatman (Anodisc 47) with an average pore size of 243 ± 20 nm and a thickness of 60 μm) by immersing the PAMs in an aqueous solution of $SnCl_2$ (0.02 M) and HCl (0.02 M) for 2 min depositing Sn^{2+} on the pore walls. The PAMs were rinsed in Nanopure water and subsequently in acetone and dried. Then the PAMs were immersed in a 0.02 M aqueous solution of $AgNO_3$ for 2 min to deposit silver seeds on the pore walls followed by a second washing step. The deposition of silver nanoparticle seeds was carried out three times to provide a high degree of particle coverage on the pore walls.

In situ Silver Nanoparticle Growth. The PAMs were immersed in 1 mL of 10 mM $AgNO_3$ and 0.5 mL of 100 mM ascorbic acid. The PAMs were removed from the solution and rinsed with nanopure water after different time periods. The silver nanoparticles assembled inside the PAMs were characterized on Hitachi-3400 and LEO 1530 SEM microscopes with gold sputtering and an operating voltage of 5−10 keV. AFM scanning was conducted to show the size and aggregation of the silver nanoparticles on a Dimension 3000-Nanoscope IIIa microscope (Digital Instruments). AFM images were collected in the tapping mode according to the procedures adapted in our lab (47, 48). AFM images of at least several different areas were obtained and the representative image was selected. Silicon nitride tips were used with spring constants of around 50 N m^{-1} and tip radii between 20−30 nm. AFM scanning was conducted with the rate of 1.0 Hz for surface areas of several micrometers across.

Raman Measurement and UV−Vis Measurement. Raman measurements were performed using a WiTec confocal Raman microscope (Alpha 300R) with an Ar^+ ion laser (λ = 514 nm) with 1 mW of intensity of the excitation source according to usual procedure (49). R6G from water was deposited on the SERS substrates and Raman spectra were collected. Each spectrum was collected with 10 s of exposure time and at least three exposures were averaged to ensure accurate spectra were recorded. Mapping images were acquired line by line with an Avalanche photodiode detector in single photon counting mode by fast imaging with a lateral resolution of approximately 250 nm and a vertical resolution of about 1 μm with a 100× objective lens. The 10 μm × 10 μm (x,y) mapping over the large area of the SERS substrate was conducted with a 50x objective lens. UV−vis spectroscopy of the SERS substrates was completed using a Craic QDI 202 spectrophotometer attached to a Leica microscope.

Acknowledgment. We thank DARPA, NSF-CBET, and the NDSEG Fellowship Program (Z.A.C.) for support and Dr. Srikanth Singamaneni for technical discussions.

REFERENCES AND NOTES

(1) Nie, S.; Emory, S. R. *Science* **1997**, *21*, 1102.
(2) Kneipp, K. *Phys. Today* **2007**, *60*, 40.

(3) Ko, H.; Singamaneni, S.; Tsukruk, V. V. *Small* **2008**, *4*, 1576.
(4) Dieringer, J. A.; Lettan, R. B., II; Scheidt, K. A.; Van Duyne, R. P. *J. Am. Chem. Soc.* **2007**, *129*, 16249.
(5) Thaxton, C. S.; Elghanian, R.; Thomas, A. D.; Stoeva, S. I.; Lee, J. S.; Smith, N. D.; Schaeffer, A. J.; Klocker, H.; Horninger, W.; Bartsch, G.; Mirkin, C. A. *Proc. Natl. Acad. Sci. U.S.A.* **2009**, *106*, 18437.
(6) Lim, D.-K.; Jeon, K.-S.; Kim, H.-M.; Nam, J.-M.; Suh, Y. D. *Nat. Mater.* **2010**, *9*, 60.
(7) Hulteen, J. C.; Treichel, D. A.; Smith, M. T.; Duval, M. L.; Jensen, T. R.; Van Duyne, R. P. *J. Phys. Chem. B* **1999**, *103*, 3854.
(8) Gunawidjaja, R.; Peleshanko, S.; Ko, H.; Tsukruk, V. V. *Adv. Mater.* **2008**, *20*, 1544.
(9) Qin, L.; Zhou, S.; Xue, C.; Atkinson, A.; Schatz, G. C.; Mirkin, C. A. *Proc. Natl. Acad. Sci. U.S.A.* **2006**, *103*, 13300.
(10) Freeman, R. G.; Grabar, K. C.; Allison, K. J.; Bright, R. M.; Davis, J. A.; Guthrie, A. P.; Hommer, M. B.; Jackson, M. A.; Smith, P. C.; Walter, D. G. *Science* **1995**, *267*, 1629.
(11) Wang, Z.; Pan, S.; Krauss, T. D.; Du, H.; Rothberg, L. J. *Proc. Natl. Acad. Sci. U.S.A.* **2003**, *100*, 8638.
(12) Gobin, A. M.; Lee, M. H.; Halas, N. J.; James, W. D.; Drezek, R. A.; West, J. L. *Nano Lett.* **2007**, *7*, 1929.
(13) Moskovits, M.; Suh, J. S. *J. Phys. Chem.* **1984**, *88*, 5526.
(14) Gunawidjaja, R.; Kharlampieva, E.; Choi, I.; Tsukruk, V. V. *Small* **2009**, *5*, 2460.
(15) Xu, P.; Mack, N. H.; Jeon, S.-H.; Doorn, S. K.; Han, X.; Wang, H. L. *Langmuir* **2010**, *26*, 8882.
(16) Xu, P.; Zhang, B.; Mack, N. H.; Doorn, S. K.; Han, X.; Wang, H. L. *J. Mater. Chem.* **2010**, *20*, 7222.
(17) Driskell, J. D.; Shanmukh, S.; Liu, Y.; Chaney, S. B.; Tang, X.-J.; Zhao, Y.-P.; Dluhy, R. A. *J. Phys. Chem. C* **2008**, *112*, 895.
(18) Han, Y.; Tan, S.; Pristinski, D.; Sukhishvili, S.; Du, H. *Adv. Mater.* **2010**, *22*, 2647.
(19) Amezcua-Correa, A.; Yang, J.; Finlayson, C. E.; Peacock, A. C.; Hayes, J. R.; Sazio, P. J. A.; Baumberg, J. J.; Howdle, S. M. *Adv. Funct. Mater.* **2007**, *17*, 2024.
(20) Ko, H.; Tsukruk, V. V. *Small* **2008**, *4*, 1980.
(21) Velev, O. D.; Tessier, P. M.; Lenhoff, A. M.; Kaler, E. W. *Nature* **1999**, *401*, 548.
(22) Velev, O. D.; Kaler, E. W. *Adv. Mater.* **2000**, *12*, 531.
(23) Haynes, C. L.; Van Duyne, R. P. *J. Phys. Chem. B* **2003**, *107*, 7426.
(24) Sundaramurthy, A.; Crozier, K. B.; Kino, G. S.; Fromm, D. P.; Schuck, P. J.; Moerner, W. E. *Phys. Rev. B* **2005**, *72*, 165409.
(25) Sweatlock, L. A.; Maier, S. A.; Atwater, H. A.; Penninkhof, J. J.; Polman, A. *Phys. Rev. B* **2005**, *71*, 235408.
(26) Chen, X.; Narayanan, R.; El-Sayed, M. A. *Chem. Rev.* **2005**, *105*, 1025.
(27) Zhao, J.; Pinchuk, A. O.; McMahon, J. M.; Li, S.; Ausman, L. K.; Atkinson, A. L. *Acc. Chem. Res. Phys.* **2008**, *41*, 1710.
(28) Sánchez-Iglesias, A.; Aldeanueva-Potel, P.; Ni, W.; Pérez-Juste, J.; Pastoriza-Santos, I.; Alvarez-Puebla, R. A.; Mbenkum, B. N.; Liz-Marzán, L. M. *Nano Today* **2010**, *5*, 21.
(29) Wang, H.-H.; Liu, C.-Y.; Wu, S.-B.; Liu, N.-W.; Peng, C.-Y.; Chan, T.-H.; Hsu, C.-F.; Wang, J.-K.; Wang, Y.-H. *Adv. Mater.* **2006**, *18*, 491.
(30) Qiu, T.; Zhang, W.; Lang, X.; Zhou, Y.; Cui, T.; Chu, P. K. *Small* **2009**, *5*, 2333.
(31) Chang, S.; Ko, H.; Singamaneni, S.; Gunawidjaja, R.; Tsukruk, V. V. *Anal. Chem.* **2009**, *81*, 5740.
(32) Saito, M.; Shibasaki, M.; Nakamura, S.; Miyagi, M. *Opt. Lett.* **1994**, *19*, 710.
(33) Lau, K. H. A.; Tan, S.; Tamada, K.; Sander, M. S.; Knoll, W. *J. Phys. Chem. B* **2004**, *108*, 10812.
(34) Lee, W.; Scholz, R.; Nielsch, K.; Gosele, U. *Angew. Chem., Int. Ed.* **2005**, *44*, 6050.
(35) Jana, N. R.; Gearheart, L.; Murphy, C. J. *Chem. Commun.* **2001**, *7*, 617.
(36) Finney, E. E.; Finke, R. G. *J. Colloid Interface Sci.* **2008**, *317*, 351.
(37) Cao, G. *Nanostructures and Nanomaterials: Synthesis, Properties, and Applications*; Imperial College Press: London, 2004.
(38) Moskovits, M.; DiLella, D. P.; Maynard, K. *Langmuir* **1988**, *4*, 67.
(39) Kelly, K. L.; Coronado, E.; Zhao, L. L.; Schatz, G. C. *J. Phys. Chem. B* **2003**, *107*, 668.
(40) Nikoobakht, B.; El-Sayed, M. A. *J. Phys. Chem. A* **2003**, *107*, 3372.
(41) Jain, P. K.; El-Sayed, M. A. *Nano Lett.* **2007**, *7*, 2854.
(42) Rechberger, W.; Hohenau, A.; Leitner, A.; Krenn, J. R.; Lamprecht, B.; Aussenegg, F. R. *Opt. Commun.* **2003**, *220*, 137.
(43) Jain, P. K.; Huang, W.; El-Sayed, M. A. *Nano Lett.* **2007**, *7*, 2080.
(44) Hildebrandt, P.; Stockburger, M. *J. Phys. Chem.* **1984**, *88*, 5935.
(45) Watanabe, H.; Hayazawa, N.; Inouye, Y.; Kawata, S. *J. Phys. Chem. B* **2005**, *109*, 5012.
(46) Ko, H.; Chang, S.; Tsukruk, V. V. *ACS Nano* **2008**, *3*, 181.
(47) Tsukruk, V. V. *Rubber Chem. Technol.* **1997**, *70*, 430.
(48) McConney, M. E.; Singamaneni, S.; Tsukruk, V. V. *Polym. Rev.* **2010**, *50*, 235.
(49) Singamaneni, S.; Gupta, M.; Yang, R.; Tomczak, M. M.; Naik, R. R.; Wang, Z. L.; Tsukruk, V. V. *ACS Nano* **2009**, *3*, 2593.

AM100758K